ACS APPLIED MATERIALS & INTERFACES

Research Article

www.acsami.org

Synthesis of Uniform α-Si_3N_4 Nanospheres by RF Induction Thermal Plasma and Their Application in High Thermal Conductive Nanocomposites

Guolin Hou,[†,‡] Benli Cheng,[†,§] Fei Ding,[†] Mingshui Yao,[∥] Peng Hu,*[,†] and Fangli Yuan*[,†]

[†]State Key Laboratory of Multi-Phase Complex Systems, Institute of Process Engineering, Chinese Academy of Sciences, Zhongguancun Beiertiao 1 Hao, Beijing 100190, P. R. China

[‡]University of Chinese Academy of Sciences, No.19A Yuquan Road, Beijing 100049, P. R. China

[§]School of Metallurgical and Ecological Engineering, University of Science & Technology Beijing, Beijing 100083, P. R. China

[∥]State Key Laboratory of Structural Chemistry, Fujian Institute of Research on the Structure of Matter, Chinese Academy of Sciences, 155 Yangqiao Road west, Fuzhou, 350002, P. R.China

ABSTRACT: In this paper, single-crystalline α-Si_3N_4 nanospheres with uniform size of ~50 nm are successfully synthesized by using a radio frequency (RF) thermal plasma system in a one-step and continuous way. All Si_3N_4 nanoparticles present nearly perfect spherical shape with a narrow size distribution, and the diameter is well-controlled by changing the feeding rate. Compact Si_3N_4/PR (PR = phenolic resin) composites with high thermal conductivity, excellent temperature stability, low dielectric loss tangent, and enhanced breakdown strength are obtained by incorporating the as-synthesized Si_3N_4 nanospheres. These enhanced properties are the results of good compatibility and strong interfacial adhesion between compact Si_3N_4 nanospheres and polymer matrix, as large amount of Si_3N_4 nanospheres can uniformly disperse in the polymer matrix and form thermal conductive networks for diffusion of heat flow.

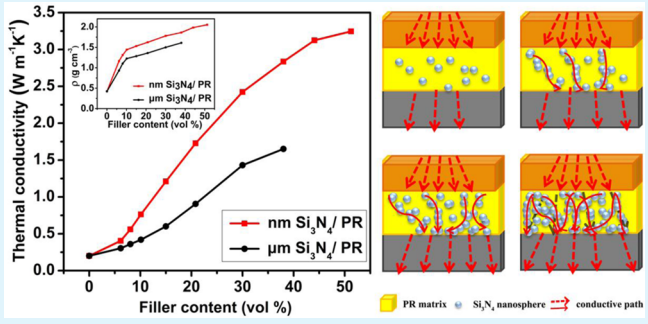

KEYWORDS: *(RF) thermal plasma, silicon nitride (α-Si_3N_4) nanoparticles, nanocomposites, thermal conductivity, dielectric loss tangent*

1. INTRODUCTION

Polymeric composites integrated with functional inorganic fillers can endow themselves with superior properties, and the comprehensive performances can be tailored by adjusting the morphology and size of the filled inorganic particles, which greatly enhance their performances in different applications.[1] A typical example is organic−inorganic composites with high thermal conductivity (κ), which are highly desired to meet the requirement of heat dissipation in electronic components as they are more and more miniaturized and integrated.[2] Inorganic materials with high thermal conductivity, such as aluminum nitride (AlN),[3−8] boron nitride (BN),[9−15] aluminum oxide (Al_2O_3),[16−18] silicon dioxide (SiO_2),[19,20] and silicon carbide (SiC),[21−23] have been introduced as fillers in polymer matrix to acquire relatively high thermal conductivity. Table 1 summarizes the previously reported thermal conductivity (κ), thermal conductivity enhancement (TCE, defined as $\lambda_{composites}/\lambda_{polymer\ matrix}$), and dielectric performances. The variation of dielectric constant $\Delta\varepsilon$ is defined as $\varepsilon_c/\varepsilon_p$, where ε_c and ε_p are the dielectric constant of the composites and polymer matrix, respectively. $\Delta\tan\delta$ is defined as $\tan\delta_c/\tan\delta_p$, and ΔE_b is defined as E_{bc}/E_{bp}, where $\tan\delta_c$, $\tan\delta_p$, E_{bc}, and E_{bp} are the dielectric loss tangent ($\tan\delta$) and the breakdown strength (E_b) of the composites and polymer matrix, respectively. As shown in Table 1, all composites show enhanced thermal conductivity by introducing different fillers into polymer. However, high thermal conductivity is accompanied by the risk of abrupt increase of dielectric loss and sharp reduction of dielectric breakdown strength.[24,25] Recently, low-dimensional carbon nanofillers such as carbon nanotube (CNT) and graphene-based polymer composites have attracted significant interest for their ultrahigh thermal conductivity.[26−28] However, compared to theoretical predictions, the CNT additives have yielded only modest increases in the thermal conductivities of polymers. This is because CNT is prone to aggregate due to the $\pi-\pi$ interaction and hydrophobic force.[27] What's worse, the poor dispersion and agglomeration also lead to high dielectric loss and low breakdown strength of the composites, which greatly restrict their practical applications. For example, the dielectric loss increases to over 10^5 at the loading of CNT of 20 wt %, and the breakdown strength drops to less than 30% of pure polymer.[29] Chen also find that small quantity addition of CNT

Received: November 21, 2014
Accepted: January 5, 2015
Published: January 5, 2015

DOI: 10.1021/am5081887
ACS Appl. Mater. Interfaces 2015, 7, 2873−2881

Table 1. Thermal Conductive and Dielectric Performances of Various Filler/Polymer

filler	matrix	loading	κ	TCE	$\Delta\varepsilon$	$\Delta\tan\delta$	ΔE_b	ref
AlN	polyimide	50 vol %	1.8	400%	225%	140%		3
AlN	epoxy	27 wt %	0.37	187%	120%	265%	80%	8
BN	epoxy	60 wt %	1.052	500%	122%	255%		14
BNNT[a]	epoxy	38 wt %	2.77	1360%	87%	18%		15
Al_2O_3	epoxy	20 wt %	0.28	138%	137%	140%	81%	18
SiO_2	epoxy	60 wt %	1.17	550%				19
SiC	epoxy	14 vol %	0.4	200%	187%	147%		22 and 23

[a]BNNT is short for BN nanotubes.

makes the breakdown strength decrease sharply.[30] Therefore, it remains a challenging task to improve the thermal conductivity without the significant reduction of dielectric breakdown strength and the abrupt increase of dielectric loss. As a structural ceramic material, silicon nitride shows great potential to improve the thermal conductivity without severe dielectric loss due to its high thermal conductivity (up to 155 W m^{-1} K^{-1})[31] and considerably low dielectric loss tangent (0.01−0.1). For example, the thermal conductivity of polyethylene composite could be greatly increased from 0.2 to 1.0 W m^{-1} K^{-1} by adding irregular micron silicon nitride particles into polymer, and the dielectric loss tangent remains less than 0.03.[32] However, further thermal conductivity improvement is limited even at high filler content due to the difficulties in achieving homogeneous dispersion and forming efficient thermal conductive paths in composite for irregular micron Si_3N_4 particles, which are produced by a traditional method using direct silicon powder nitriding in a fluidized bed or quartz tube furnace.[33]

To overcome these limitations, the introduction of nanosized particles into polymer matrix had been proposed, and nanocomposites with relatively high performances were obtained with the use of nano-Si_3N_4.[34] Although significant advances have been made, the realization of high thermal conductivity and low dielectric loss nanocomposites remains a challenging task. One of the most challenging issues for application of nano-Si_3N_4 is the strong tendency of nanosized particles to agglomerate because of their high surface energy, which results in phase separation from the polymer host matrix and high defect density.[35] Some nanoparticle-filled polymer composites contain a number of loosened clusters, which inhibit the forming of thermally conductive paths and cut off the diffusion of heat flow, leading to even worse performance (e.g., low thermal conductivity and high dielectric loss) than that of conventional particle/polymer systems.[36] Nanoparticles with definite morphology, such as one-dimensional (1D) structure, have been confirmed to form efficient thermally conductive paths in polymer matrix and greatly increase their thermally conductive properties.[37] However, in practical application, 1D structure still cannot get rid of the adverse effect of agglomeration because of the large aspect ratio, which greatly limits the filler content and restricts their applications in some fields. Compact nanoparticles with smooth surface and isotropic structure (especially spherical shape) are apt to uniformly disperse in polymer matrix and form thermally conductive paths at the same time, which can improve the thermal conductivity of composites without increasing the dielectric loss and reducing the breakdown strength. However, to the best of our knowledge, the utility of Si_3N_4 nanospheres as fillers to improve the thermal conductivity and reduce the dielectric loss of composites has not been reported.

In this paper, a novel strategy has been reported to synthesize highly uniform Si_3N_4 nanospheres a in one-step and efficient way by using the radio frequency induction thermal plasma (RF-plasma) system. The as-obtained particles present nearly perfect compact spherical shape with a narrow size distribution. Specifically, the Si_3N_4/PR (PR = phenolic resin) composites incorporating spherical Si_3N_4 nanoparticles show high thermal conductivity and low dielectric loss tangent. These desirable property enhancements are attributed to the uniform spherical structure of the Si_3N_4 nanospheres, which could not only enhance the dispersion in polymer matrix but also improve the formation of efficient thermally conductive paths.

2. EXPERIEMENTS

2.1. Scheme of RF Induction Thermal Plasma Setup. A schematic of the plasma jet reactor is shown in Figure 1. The

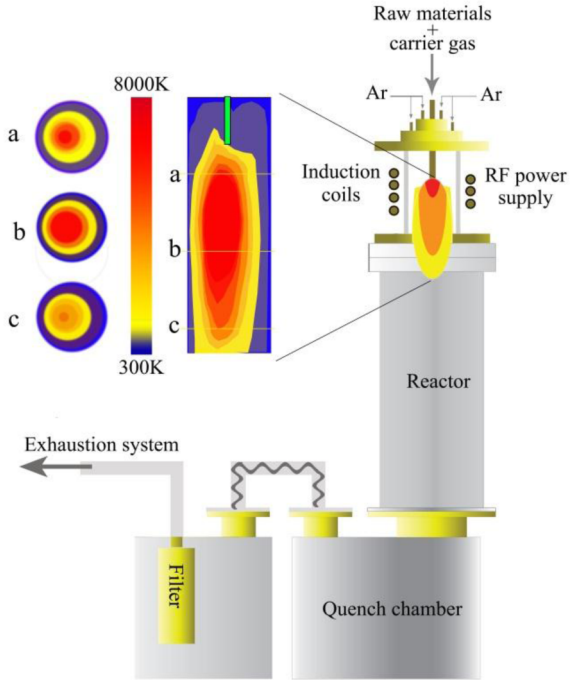

Figure 1. Schematic illustration of the RF induction thermal plasma processing system setup and temperature distribution of the plasma jet.

experimental setup consists of an RF generator (10 kW, 4 MHz), a swirl-stabilized plasma torch, a cylindrical reactor, a quench/collection chamber, a particle feeder system, a powder-collecting filter, and an off-gas exhaust system. The plasma torch consists of a quartz tube to confine thermal plasma and a water-cooled induction coil to couple its electromagnetic energy to thermal plasma. Argon (Ar, 99.9%) was used as the plasma gas and the quenching gas. When the RF thermal

DOI: 10.1021/am5081887
ACS Appl. Mater. Interfaces 2015, 7, 2873−2881

plasma is running, the central gas is injected continually to stabilize the plasma jet, and the sheath gas is to protect the quartz tube from the high temperature of the discharge.

2.2. Synthesis of Si_3N_4 Nanospheres. For Si_3N_4 nanosphere synthesis, the starting powders of large silicon nitride (5−10 μm, irregular bulk) were delivered into the plasma flame by the carrier gas (NH_3, 99.9%) in a continuous way. The evaporation reaction occurred in the plasma jet and was cooled by the quenching gas, and products were obtained in the collection chamber. The synthesis of nanoparticles by thermal plasmas is an intricate heat and mass transfer process that involves a phase conversion in a few tens of milliseconds, as well as interactions among the thermo fluid field, the induced electromagnetic field, and the particle concentration field, all of which are described by numerous variables. Thus, the parameters for plasma processing are very important for stable operation; they are given in Table 2 in detail.

Table 2. Detailed Parameters for RF Induction Thermal Plasma Processing

parameters	values
plasma power	10 kW
central gas, argon	0.8 m^3 h^{-1}
sheath gas, argon	2.0 m^3 h^{-1}
carrier gas, NH_3	0.1−0.6 m^3 h^{-1}
cooling gas, argon	0−2 m^3 h^{-1}
negative pressure	50−100 mm H_2O
powder feeding rate	1−10 g min^{-1}

2.3. Preparation Process of Si_3N_4/PR Composites. A certain proportion of nanoparticles was dispersed into ethanol and ultrasonicated for 1 h at room temperature. Then, the nanoparticle/alcohol suspension was added into the liquid PR step by step under stirring, followed by rapid mechanical stirring for 1 h at 60 °C to ensure good homogeneity and remove the alcohol entirely. Then, hexamethylenetetramine was added under the continued rapid mechanical stirring. Subsequently, the collosol was vacuum degassed for 30 min at 80 °C. Then, the mixture was poured into a homemade stainless-steel mold and cured in an oven at 130 °C for 2 h. Finally, Si_3N_4/PR composite was achieved after demolding when the mold cooled to room temperature.

2.4. Characterization. The phase and crystal structure of obtained products were characterized by X-ray diffraction (XRD, Philips X' Pert PRO MPD) operated at 40 kV and 30 mA with Cu Kα radiation. The morphology and structure of the products were observed by transmission electron microscope (TEM, JEOL JEM-2100), high-resolution TEM (HRTEM), and field-emission scanning electron microscope (FESEM, JSM-6700F) equipped with an energy dispersive X-ray spectrometer (EDX). A BET surface area analyzer (Micrometric, ASAP 2010) was used to measure the surface area and average size of the produced Si_3N_4 nanoparticles. The size distribution of as-synthesized Si_3N_4 spheres was measured and figured out by Nanomeasurer program. Thermal gravimetric analyses (TGA) and differential scanning calorimetry (DSC) of Si_3N_4/PR composites were performed with a TG-209 F3 instrument (NETZSCH, Germany) at a heating rate of 10 °C min^{-1} under the nitrogen atmosphere. Thermal conductivities of the composites were measured with LFA 427 Nanoflash (NETZSCH, Germany) according to ASTM E1461, using the measured heat capacity and thermal diffusivity, with separately entered density data. Samples were prepared in cylindrical shape of 12.5 mm in diameter and 3.0 mm in thickness. The dielectric and electrical properties were measured using an Agilent 4294A impedance analyzer in the frequency range from 1 kHz to 10 MHz. The breakdown strength was conducted using a direct current dielectric strength tester (DH, Shanghai Lanpotronics Co., China) in a voltage ramp rate of 2 V s^{-1} at room temperature.

3. RESULTS AND DISCUSSION

3.1. Characterization. After the experiment, large-scale, white to gray-white, ultrafine Si_3N_4 powders were obtained in the collector. Figure 2 displays the typical XRD pattern of the

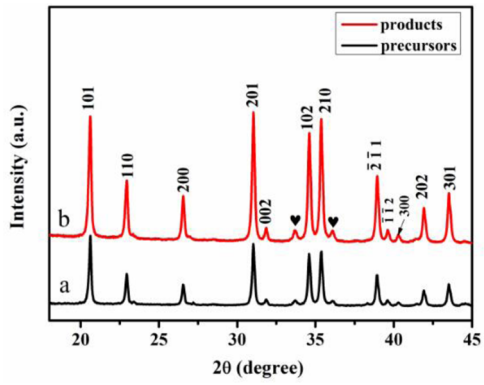

Figure 2. Typical XRD patterns of the Si_3N_4 precursors (a) and products (b) obtained at typical plasma parameters (input power of 10 kW, powder feeding rate of 3.78 g min^{-1}, carrier gas of 0.6 m^3 h^{-1}, and quenching gas of 2 m^3 h^{-1}).

Si_3N_4 precursors and products. No disintegration of the chemical structure was observed after the plasma synthesis process, except the increased intensity of diffraction peaks, indicating the high crystallization of the products compared to that of the starting materials. The obtained products could be readily indexed to hexagonal structural α-Si_3N_4 (JCPDS No. 01−076−1407, space group: $P31c$, lattice constants: $a = b =$ 7.7523 Å, c = 5.6198 Å and $\alpha = \beta = 90°$, $\gamma = 120°$) with a small amount of hexagonal β-Si_3N_4 (JCPDS No. 01−082−0699, space group: $P63$, lattice constants: $a = b$ = 7.6064 Å, c = 2.9091 Å and $\alpha = \beta = 90°$, $\gamma = 120°$). No peaks corresponding to Si or silicon oxide were observed in the XRD patterns of as-synthesized products.

The morphological and structural information of as-synthesized products provided by FESEM and TEM are shown in Figure 3. The raw materials display irregular shape with particle size beyond micrometers as shown in Figure 3a. After plasma synthesis process, the well-defined monodisperse nanospheres with size of ∼50 nm was dominant in as-synthesized products, and no particles with other shape were obtained from the FESEM images in Figure 3b. In addition, the spherical particle was observed to possess smooth surface from inset of Figure 3b. The composition of as-prepared nanospheres (sample in Figure 3b) could be further evidenced by EDS spectroscopy (Figure 3c). It indicates the Si_3N_4 nanocrystals mainly composed of N and Si with ratio of 1.30, close to the theoretic stoichiometric ratio in Si_3N_4 crystal. In addition, very small O peaks were detected in the EDX spectroscopy, which may be attributed to the surface oxidization of particles after the experiment. The Si_3N_4 nanospheres show an extremely narrow size distribution of 30−50 nm, and no agglomeration was observed according to size distribution analysis in Figure 3d. Note that the specific surface area of synthesized products is measured to be 43.75 m^2 g^{-1}, which is consistent with the theoretical calculated value of spherical particles with the diameter of 40 nm. It further confirms that perfect nanospheres with a narrow size distribution were obtained. The detailed structural analyses of Si_3N_4 nanospheres were performed using TEM analysis in

DOI: 10.1021/am5081887
ACS Appl. Mater. Interfaces 2015, 7, 2873−2881

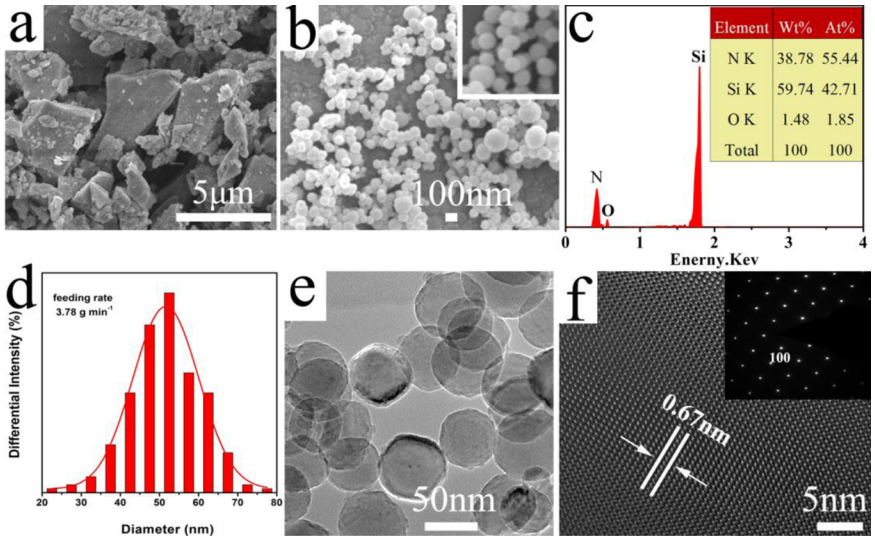

Figure 3. FESEM images of (a) raw powders and (b) as-prepared Si_3N_4 nanoparticles, (c) the EDS spectrum, (d) particle size distribution, (e) TEM image, and (f) lattice-resolved HRTEM image of as-prepared nanoparticles (inset shows the corresponding SAED pattern).

Figure 3e, which clearly displays the uniform spherical shape, which is the same as SEM observation. HRTEM (Figure 3f) shows a clean and perfect crystalline structure, indicating the single-crystalline structure of the nanosphere. The measured lattice spacing of adjacent lattice planes is 0.67 nm, corresponding to (100) plane of α-Si_3N_4 crystal. It, together with SAED pattern, confirms single-crystalline structure of as-synthesized Si_3N_4 nanoparticles.

In plasma synthesis process, the particle size of obtained nanospheres could be well-adjusted by controlling the parameters. Experiments were further conducted to evaluate the effect of vapor concentration on particle size by changing the initial feed rate. Figure 4 exhibits the typical SEM and TEM

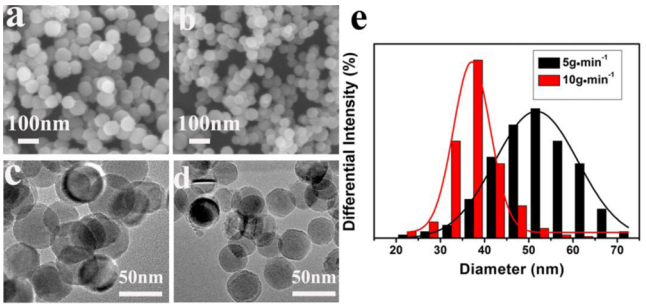

Figure 4. SEM images of the α-Si_3N_4 nanospheres synthesized at different feeding rates: (a) 5 g min^{-1} and (b) 10 g min^{-1}, and TEM images of (c) 5 g min^{-1} and (d) 10 g min^{-1}; (e) particle size distribution with different feeding rates.

images of nanospheres obtained at different feeding rates. When raw powders were injected at a rate of 5 g min^{-1}, uniform nanospheres with an average diameter of 52 nm were obtained. However, the average diameter decreased to ~35 nm at the feeding rate of 10 g min^{-1} (showed in Figure 4a–d). It reveals that low supersaturation results in larger particle size. In vapor synthesis process, supersaturation plays a key role in the particle size and distribution.[38] Under high supersaturations of chemical species, nucleation rate increased, and large numbers of nuclei formed and exhausted most of the nutrient, leading to undernutrition for nuclei growth process. Together with the homogeneous growth, it results in small particle size. In contrast, low supersaturation results in larger particle size. Importantly, all the products reveal extremely narrow size distribution as shown in Figure 4e.

3.2. Growth Mechanism of α-Si_3N_4 Nanospheres. In thermal plasma synthesis, it is an intricate heat and mass transfer process that involves phase conversion, interactions among thermo fluid field, electromagnetic field, and particle concentration field.[39,40] The growth of nanoparticles in plasma includes mainly three processes: decomposition process, cooling process, and nanoparticle growth process. The whole process started with the decomposition of precursor Si_3N_4 by virtue of the high enthalpy of the plasma, as silicon nitride has no fixed melting point. During the rapid heating process, silicon nitride split into Si(g) and N*(g) (high activity), and NH_3 split into H(g) and N*(g) at the same time. Subsequently, vapor chemical species transported to the tail or fringe of the plasma where the temperature decreased drastically, and the recombination of Si(g) and N*(g) occurred to form silicon nitride molecule rapidly. In the RF-enhanced chemical vapor deposition reaction system, extremely high degree of supersaturation tends toward a homogeneous nucleation;[40] all growing crystal faces had great kinks and corresponding growth rates. During the rapid quenching process, the freshly formed nucleuses were frozen in growth process and tended to form spherical shape as it possesses the minimum surface energy.[41,42] All possible reactions involved above are listed below:

$$Si_3N_4(s) \rightarrow Si(g) + N_2(g) \quad (1)$$

$$NH_3 \rightarrow N^* + H_2(g) \quad (2)$$

$$N_2(g) \rightarrow N^* \quad (3)$$

$$Si(g) + N^* \rightarrow Si_3N_4(g) \rightarrow Si_3N_4(s) \quad (4)$$

On the basis of the results and discussions above, the overall growth process of α-Si_3N_4 nanospheres can be schematically illustrated in Figure 5.

3.3. Thermal Stability of Si_3N_4/PR Composite. It has been confirmed that the thermally conductive properties of the polymer nanocomposites are closely associated with the

DOI: 10.1021/am5081887
ACS Appl. Mater. Interfaces 2015, 7, 2873–2881

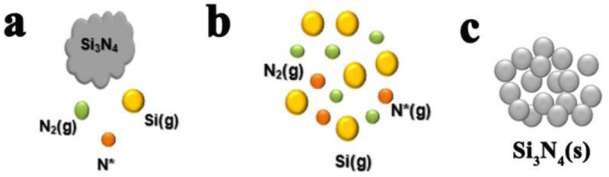

Figure 5. Schematic illustration of nanosphere growth process: (a) decomposition process, (b) cooling process, and (c) nanoparticle growth process.

dispersion and interface adhesive between fillers and matrix.[43,44] Therefore, useful information about the Si_3N_4/PR interface was achieved by analyzing the thermal property of the nanocomposites. The thermal stability of Si_3N_4/PR composites investigated by TG and differential thermal analysis (DTA) measurements are shown in Figure 6. Pure PR and Si_3N_4/PR

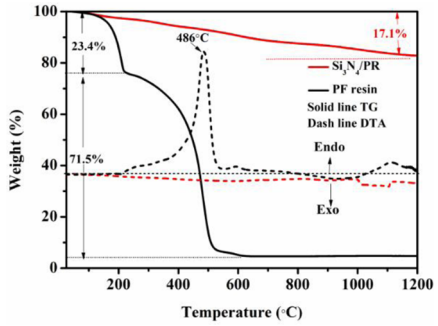

Figure 6. TG and DTA curves of 38 vol % Si_3N_4/PR composite and pure PR under N_2 atmosphere at the heating rate of 10 °C min^{-1}.

composites display almost distinct degradation profiles. The TG curve of pure PR can be divided into three phases obviously, which is similar to previous reports.[45−47] In the first stage from room temperature to 225 °C, small terminal groups of the cured resin were removed, accompanied by the formation of additional cross-links as a result of condensation reactions.[47] And in the second degradation stage (225−500 °C), the methylene bridges were decomposed into methyl groups then yielded phenol and cresol monomers. At the same time, small molecules such as CO, CO_2, CH_4, and H_2O were released, accompanied by a significant weight loss.[48] The phenol groups degraded in the third stage (500−1200 °C) and completely volatilized at higher temperature of 600 °C. However, for Si_3N_4/PR composites, no obvious decomposition peaks were observed within the whole heating process, and only 17.7 wt % weight was lost until 1200 °C, suggesting that the existence of Si_3N_4 nanospheres significantly improve the thermal stability of pure PR. This dramatic improvement of thermal stability is closely related to the interfacial interaction between nanoparticles and polymer matrix.[49,50] With nanoscale and smooth spherical morphology, Si_3N_4 nanospheres disperse uniformly in the polymer matrix, and a large fraction of atoms of Si_3N_4 nanospheres reside at the interface, leading to a strong particle/matrix interfacial interaction, which is an effective way to restrict the thermal motion of polymer chains and improve the thermal stability.[51]

3.4. Thermal Conductive and Dielectric Properties of Si_3N_4/PR Composite. Figure 7 shows the thermal conductivity curves of the composites incorporated with irregular micron silicon nitride and nanospherical silicon nitride. All

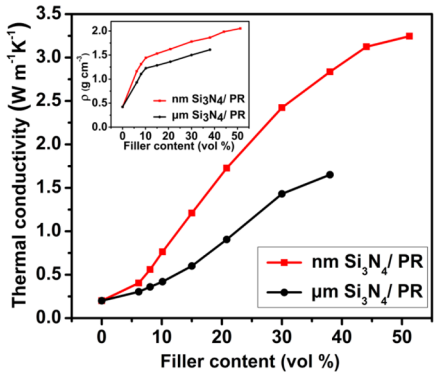

Figure 7. Thermal conductivity curve of Si_3N_4/PR composites.

composites show an enhancement in thermal conductivity with the increase of Si_3N_4 fillers, and the thermal conductivity curve of Si_3N_4/PR composite exhibits sigmoidal plot with overall shape. Conductive property improves slowly at low filler content and then rapidly increased when the filler content is further increased. However, when the filler content is greater than a certain extent, the increase of thermal conductivity slows down. Importantly, the nano-Si_3N_4 composite exhibits superior thermal conductivity compared to that of micron-Si_3N_4 composite, especially at high filler content. For example, with 38 vol % filler content, the thermal conductivity of nano-Si_3N_4/PR composite is 2.8 W m^{-1} K^{-1}, almost 2 times that of micron-Si_3N_4/PR composite (~1.5 W m^{-1} K^{-1} and it is the highest value) and 14 times that of pure PR (0.2 W m^{-1} K^{-1}). When the filler content continually increases to 45 vol %, the thermal conductivity of nano-Si_3N_4/PR composite increases to 3.12 W m^{-1} K^{-1}. More importantly, it can increase to 3.25 W m^{-1} K^{-1} when the filler content further increases to 50 vol %, almost 16 times that of pure PR.

The typical thermal conductivity change of obtained nano-Si_3N_4/PR composite could be well-explained by the distribution state of nanoparticles in the organic matrix. At low filler content, Si_3N_4 nanospheres are isolated like "islands" in matrix (as shown in Figure 8b), which inhibits the formation of thermal conductive paths and stops the diffusion of heat flow, and thus the nanospheres show low conductivity. With the increase of fillers in Figure 8c, some Si_3N_4 nanospheres begin to connect with each other but are still isolated by matrix with low

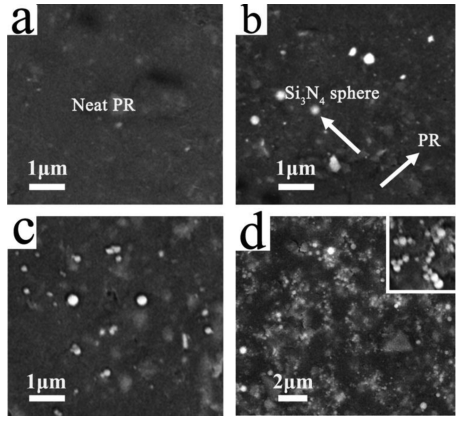

Figure 8. SEM images of fracture surface of (a) neat PR and Si_3N_4/PR composites with different filler content of (b) 3 vol %, (c) 10 vol %, (d) 38 vol %.

DOI: 10.1021/am5081887
ACS Appl. Mater. Interfaces 2015, 7, 2873−2881

thermal conductivity, resulting in the slow increase of overall conductivity. When the filler content reaches to a certain critical value, conductive particles form dense packing and connect into thermal conductive paths (as shown in Figure 8d). As a result, the resin layer between nanoparticles becomes thinner, and the thermal resistance decreases. Once it happens, the thermal conductivity of composite will be dominated by high thermal conductive additives and increase remarkably.[52] By continually increasing the filler content, conductive paths are strengthened, and the thermal conductivity remains steadily increasing. However, when the filler content is greater than 45 vol %, the thermal resistance along the conductive paths caused by nanoparticle surface effect becomes an unneglected factor, leading to the increase of thermal conductivity slowing down.

On the basis of the above results and discussions, the thermal conductivity mechanism of composites can be schematically illustrated in Figure 9. Generally, achieving dense packing and forming thermally conductive paths for diffusion of heat flow are the key points to obtain high thermal conductivity, as the thermal conductivity of resin matrix is very low (0.2 W m^{-1} K^{-1}). Specially, the thermal conductivity of air existing in the gap of resin matrix is only 0.026 W m^{-1} K^{-1},[7,35] which seriously restricts the diffusion of heat flow and leads to an overall relatively low thermal conductivity. With intrinsic high thermal conductivity (up to 155 W m^{-1} K^{-1}),[31] near-perfect spherical morphology, nanoscale size distribution, and smooth surface, the as-synthesized Si_3N_4 nanospheres have a unique advantage in achieving dense packing and forming thermal conductive paths.[53] In addition, compared to micron irregular particles and granular aggregate, larger interface would be induced as the Si_3N_4 nanospheres are uniformly dispersed in the polymer matrix, resulting in a strong particle/matrix interfacial interaction, which has been proved to be an effective way to decrease the interfacial thermal resistance and improve the thermal conductivity.[51,52]

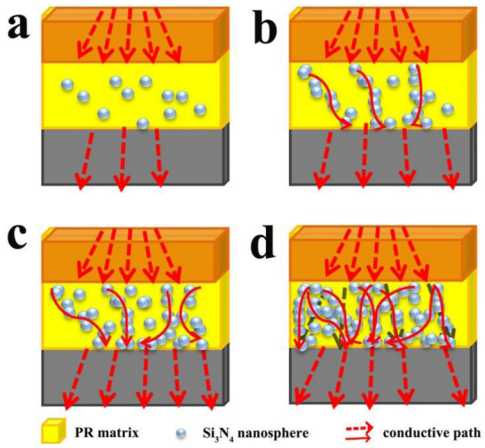

Figure 9. Model of heat dissipation.

The frequency dependence of dielectric properties of pure PR and Si_3N_4/PR nanocomposites with different filler contents were measured at room temperature (Figure 10). The dielectric constants of Si_3N_4/PR composites increase steadily with the increasing of fillers and slightly decrease as the frequency increases as shown in Figure 10a. At low frequency (<10 kHz), the dielectric constants of composites are lower than that of pure PR, and higher than that of pure PR at high frequency, which shows an overall stable and low trend over the frequency range from 1 kHz to 10 MHz. For example, at a volume fraction of Si_3N_4 nanospheres of 38%, the dielectric constant of composite remains at a low value of six over the frequency range from 1 kHz to 10 MHz. Generally, the increase in dielectric constant of composites is mainly ascribed to interfacial polarization explained on the basis of percolation theory.[54−56] Large interfacial areas are induced as Si_3N_4 nanospheres are uniformly dispersed in the polymer matrix, leading to a high degree of interfacial polarization, resulting in the dielectric constant increasing. At high frequencies, the decrease of dielectric constant is due to the relaxation of PR dipole polarization.[57] That is, orientation polarization of dipoles cannot follow with external electric field gradually and leads to the decrease of dielectric constant.

Figure 10b shows the frequency dependence of dielectric loss tangent (tan δ) of Si_3N_4/PR nanocomposites and pure PR. All nanocomposites show decreased tan δ in comparison with the pure PR, and the tan δ of the nanocomposites decreases with the increasing of Si_3N_4 loading, which is similar to Perry's results.[35] For example, at the frequency of 1 kHz, the tan δ value decreases from 0.8 for pure PR to 0.4 for 3 vol % Si_3N_4/PR nanocomposites, 0.36 for 10 vol % Si_3N_4/PR, 0.29 for 20 vol % Si_3N_4/PR, and 0.09 for 38 vol % Si_3N_4/PR. Dielectric loss generally originates from three distinct aspects: conduction (transport-related loss), movement of molecular dipoles (dipolar loss), and space charge (interfacial polarization contribution).[58,59] It is widely accepted that tan δ is mainly

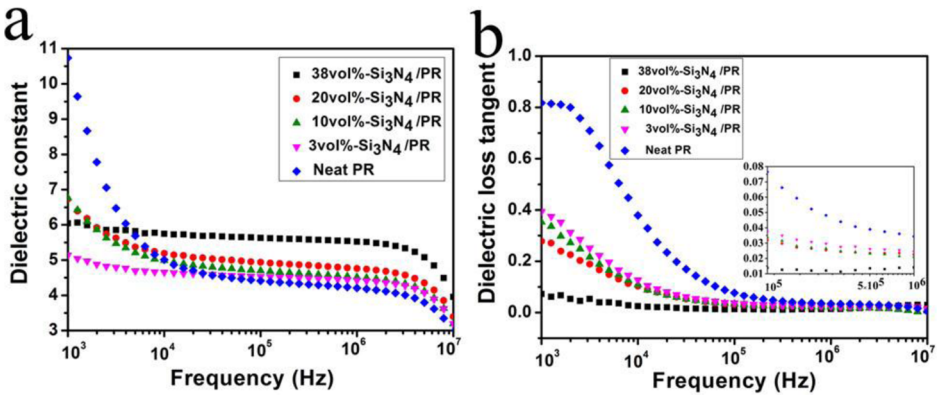

Figure 10. Frequency dependence of (a) dielectric constant and (b) dielectric loss tangent of neat PR and Si_3N_4/PR composites with different filler contents.

DOI: 10.1021/am5081887
ACS Appl. Mater. Interfaces 2015, 7, 2873−2881

associated with interfacial polarization at low frequency, whereas dipolar relaxation process is dominant at high frequencies. At low frequency, the smooth surface and compact spherical morphology improve the dispersion of Si_3N_4 nanospheres and enhance the interfacial adhesion between Si_3N_4 nanospheres and PR, which further suppresses the accumulation of the space charge within the nanocomposites and the movement of molecular dipoles,[55] leading to low tan δ. At high frequency, the low tan δ is ascribed to the weakness of dipole polarization of PR as the filler content increases (i.e., the content of PR is reduced). As a result, the tan δ tends to remain a stable and low value (less than 0.1) over the frequency range from 1 kHz to 10 MHz, especially when the content of Si_3N_4 nanospheres reaches to 38 vol %.

In practical applications, high breakdown strength (E_b) is also an important factor, as it determines the operating electric field.[60] Figure 11 shows the E_b of Si_3N_4/PR composites with

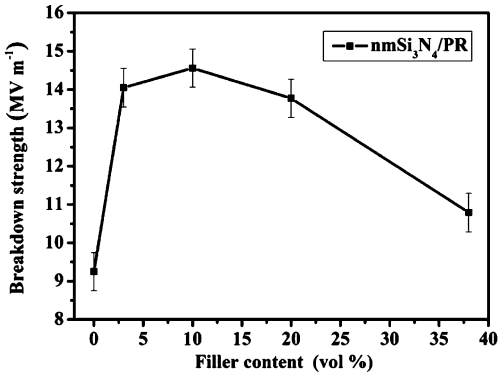

Figure 11. Breakdown strength of Si_3N_4/PR composites with different filler content of Si_3N_4 nanospheres.

different filler content. It is found that the E_b of Si_3N_4/PR nanocomposite increases at low loading of Si_3N_4 nanospheres. For example, with 3 vol % filler content, The E_b value of the nanocomposite is 14.05 MV m^{-1}. Importantly, it can increase to 14.56 MV m^{-1} when the filler content further increases to 10 vol %, which represents a 57% increase over the E_b of pure matrix (9.25 MV m^{-1}). However, the E_b gradually decreases when the filler content is over 10 vol %. At low loading, Si_3N_4 nanospheres act as scattering centers in the composites and increase the charge scattering, leading to the increase of E_b.[61,62] However, at high loading, the decrease of E_b is due to the electrical pathway formation and the electric field enhancement near the interface, as the electric properties between fillers and polymer are different.[63] Note that even at high filler content of 38 vol %, the E_b value of the nanocomposite is 10.79 MV m^{-1}, which is still higher than that of pure PR.

4. CONCLUSION

Large-scale, single-crystalline α-Si_3N_4 nanospheres with controlled size distribution have been synthesized via a simple, continuous, and one-step way by using a radio frequency (RF) thermal plasma system. The obtained nanospheres display perfect spherical shape with smooth surface. The experimental results reveal that the degree of supersaturation in the reactor, controlled mainly by the initial vapor concentration, plays a key role in the particle size of obtained products. With using the as-synthesized Si_3N_4 nanospheres, compact nanocomposites with uniform dispersion are obtained, which exhibit high thermal conductivity, good thermal stability, low dielectric loss tangent, and enhanced breakdown strength. With 50 vol % Si_3N_4 nanospheres, the thermal conductivity of nanocomposites is 3.25 W m^{-1} K^{-1}, almost 16 times that of pure PR. More importantly, the dielectric loss of nanocomposite continuously decreases with the increasing of Si_3N_4 nanospheres and maintains a stable and low value (less than 0.1) over the frequency range from 1 kHz to 10 MHz. And the breakdown strength of the nanocomposite is enhanced even at high filler content of 38 vol %. These superior properties are attributed to the uniform spherical structure of the nanosized Si_3N_4 fillers, which enhance the dispersion in polymer matrix and improve the formation of efficient thermal conductive paths.

AUTHOR INFORMATION

Corresponding Authors

*E-mail: pengh@home.ipe.ac.cn.
*E-mail: flyuan@home.ipe.ac.cn. Fax: +86-10-62561822. Phone: +86-10-82544974.

Notes

The authors declare no competing financial interest.

REFERENCES

(1) Godovsky, D. Y. Device Applications of Polymer-Nanocomposites. *Adv. Polym. Sci.* **2000**, *153*, 163−205.
(2) Chung, D. D. *Applied Materials Science: Applications of Engineering Materials in Structural, Electronics, Thermal, and Other Industries;* CRC Press: Boca Raton, FL, 2010.
(3) Wang, J. J.; Yi, X. S. Preparation and the Properties of PMR-Type Polyimide Composites with Aluminum Nitride. *J. Appl. Polym. Sci.* **2003**, *89*, 3913−3917.
(4) Yu, S.; Hing, P.; Hu, X. Thermal Conductivity of Polystyrene−Aluminum Nitride Composite. *Composites, Part A* **2002**, *33*, 289−292.
(5) Lee, G. W.; Park, M.; Kim, J.; Lee, J. I.; Yoon, H. G. Enhanced Thermal Conductivity of Polymer Composites Filled with Hybrid Filler. *Composites, Part A* **2006**, *37*, 727−734.
(6) Xie, S. H.; Zhu, B. K.; Li, J. B.; Wei, X. Z.; Xu, Z. K. Preparation and Properties of Polyimide/Aluminum Nitride Composites. *Polym. Test.* **2004**, *23*, 797−801.
(7) Bae, J. W.; Kim, W.; Cho, S. H.; Lee, S. H. The Properties of AlN-Filled Epoxy Molding Compounds by the Effects of Filler Size Distribution. *J. Mater. Sci.* **2000**, *35*, 5907−5913.
(8) Peng, W.; Huang, X.; Yu, J.; Jiang, P.; Liu, W. Electrical and Thermophysical Properties of Epoxy/Aluminum Nitride Nanocomposites: Effects of Nanoparticle Surface Modification. *Composites, Part A* **2010**, *41*, 1201−1209.
(9) Zhou, W. Y.; Qi, S. H.; An, Q. L.; Zhao, H. Z.; Liu, N. L. Thermal Conductivity of Boron Nitride Reinforced Polyethylene Composites. *Mater. Res. Bull.* **2007**, *42*, 1863−1873.
(10) Yung, K. C.; Liem, H. Enhanced Thermal Conductivity of Boron Nitride Epoxy-Matrix Composite Through Multi-Modal Particle Size Mixing. *J. Appl. Polym. Sci.* **2007**, *106*, 3587−3591.
(11) Hill, R. F.; Supancic, P. H. Thermal Conductivity of Platelet-Filled Polymer Composites. *J. Am. Ceram. Soc.* **2002**, *85*, 851−857.
(12) Kemaloglu, S.; Ozkoc, G.; Aytac, A. Properties of Thermally Conductive Micro and Nano Size Boron Nitride Reinforced Silicon Rubber Composites. *Thermochim. Acta* **2010**, *499*, 40−47.
(13) Zhou, W. Y.; Qi, S. H.; Zhao, H. Z.; Liu, N. L. Thermally Conductive Silicone Rubber Reinforced with Boron Nitride Particle. *Polym. Compos.* **2007**, *28*, 23−28.
(14) Gu, J.; Zhang, Q.; Dang, J.; Xie, C. Thermal Conductivity Epoxy Resin Composites Filled with Boron Nitride. *Polym. Adv. Technol.* **2012**, *23*, 1025−1028.
(15) Huang, X.; Zhi, C.; Jiang, P.; Golberg, D.; Bando, Y.; Tanaka, T. Polyhedral Oligosilsesquioxane Modified Boron Nitride Nanotube

DOI: 10.1021/am5081887
ACS Appl. Mater. Interfaces 2015, 7, 2873−2881

Based Epoxy Nanocomposites: An Ideal Dielectric Material with High Thermal Conductivity. *Adv. Funct. Mater.* **2013**, *23*, 1824−1831.
(16) Shimazaki, Y.; Hojo, F.; Takezawa, Y. Highly Thermoconductive Polymer Nanocomposite with a Nanoporous alpha-Alumina Sheet. *ACS Appl. Mater. Interfaces* **2009**, *1*, 225−227.
(17) Song, S. H.; Katagi, H.; Takezawa, Y. Study on High Thermal Conductivity of Mesogenic Epoxy Resin with Spherulite Structure. *Polymer* **2012**, *53*, 4489−4492.
(18) Yu, J.; Huo, R.; Wu, C.; Wu, X.; Wang, G.; Jiang, P. Influence of Interface Structure on Dielectric Properties of Epoxy/Alumina Nanocomposites. *Macromol. Res.* **2012**, *20*, 816−826.
(19) Sun Lee, W.; Yu, J. Comparative Study of Thermally Conductive Fillers in Underfill for the Electronic Components. *Diamond Relat. Mater.* **2005**, *14*, 1647−1653.
(20) Gonon, P.; Sylvestre, A.; Teysseyre, J.; Prior, C. Combined Effects of Humidity and Thermal Stress on the Dielectric Properties of Epoxy-Silica Composites. *Mater. Sci. Eng., B* **2001**, *83*, 158−164.
(21) Hussain, M.; Oku, Y.; Nakahira, A.; Niihara, K. Effects of Wet Ball-Milling on Particle Dispersion and Mechanical Properties of Particulate Epoxy Composites. *Mater. Lett.* **1996**, *26*, 177−184.
(22) Zhou, T.; Wang, X.; Gu, M.; Xiong, D. Study on Mechanical, Thermal and Electrical Characterizations of Nano-SiC/Epoxy Composites. *Polym. J.* **2008**, *41*, 51−57.
(23) Zhou, T.; Wang, X.; Liu, X.; Xiong, D. Improved Thermal Conductivity of Epoxy Composites Using a Hybrid Multi-Walled Carbon Nanotube/Micro-SiC Filler. *Carbon* **2010**, *48*, 1171−1176.
(24) Yang, W.; Yu, S.; Sun, R.; Ke, S.; Huang, H.; Du, R. Electrical Modulus Analysis on the Ni/CCTO/PVDF System near the Percolation Threshold. *J. Phys. D: Appl. Phys.* **2011**, *44*, 475305.
(25) Dang, Z.; Shen, Y.; Fan, L.; Cai, N.; Nan, C.; Zhao, S. Dielectric Properties of Carbon Fiber Filled Low-Density Polyethylene. *J. Appl. Phys.* **2003**, *93*, 5543−5545.
(26) Kim, P.; Shi, L.; Majumdar, A.; McEuen, P. Thermal Transport Measurements of Individual Multiwalled Nanotubes. *Phys. Rev. Lett.* **2001**, *87*, 215502.
(27) Marconnet, A. M.; Yamamoto, N.; Panzer, M. A.; Wardle, B. L.; Goodson, K. E. Thermal Conduction in Aligned Carbon Nanotube−Polymer Nanocomposites with High Packing Density. *ACS Nano* **2011**, *5*, 4818−4825.
(28) Ngo, Q.; Cruden, B. A.; Cassell, A. M.; Sims, G.; Meyyappan, M.; Li, J.; Yang, C. Y. Thermal Interface Properties of Cu-Filled Vertically Aligned Carbon Nanofiber Arrays. *Nano Lett.* **2004**, *4*, 2403−2407.
(29) Wu, C.; Huang, X.; Wu, X.; Xie, L.; Yang, K.; Jiang, P. Graphene Oxide-Encapsulated Carbon Nanotube Hybrids for High Dielectric Performance Nanocomposites with Enhanced Energy Storage Density. *Nanoscale* **2013**, *5*, 3847−3855.
(30) Chen, Y.; Lin, B.; Zhang, X.; Wang, J.; Lai, C.; Sun, Y.; Liu, Y.; Yang, H. Enhanced Dielectric Properties of Amino-Modified-CNT/Polyimide Composite Films with a Sandwich Structure. *J. Mater. Chem. A* **2014**, *2*, 14118−14126.
(31) Watari, K.; Hirao, K.; Brito, M. E.; Toriyama, M.; Kanzaki, S. Hot Isostatic Pressing to Increase Thermal Conductivity of Si_3N_4 Ceramics. *J. Mater. Res.* **1999**, *14*, 1538−1541.
(32) Zhou, W. Y.; Wang, C. F.; Ai, T.; Wu, K.; Zhao, F. J.; Gu, H. Z. A Novel Fiber-Reinforced Polyethylene Composite with Added Silicon Nitride Particles for Enhanced Thermal Conductivity. *Composites, Part A* **2009**, *40*, 830−836.
(33) Wang, F.; Qin, X. F.; Jin, G. Q.; Guo, X. Y. Temperature-Controlled Synthesis of Si_3N_4 Nanomaterials via Direct Nitridation of Si Powders. *Phys. E* **2010**, *42*, 2033−2035.
(34) Yan, H.; Zhang, M.; Liu, C.; Zhang, J. Nano-Si_3N_4/Epoxidized Silane/Cyanate Ester Composites for Electronic Packaging. *Polym. Bull.* **2013**, *70*, 2923−2933.
(35) Kim, P.; Doss, N. M.; Tillotson, J. P.; Hotchkiss, P. J.; Pan, M. J.; Marder, S. R.; Li, J. Y.; Calame, J. P.; Perry, J. W. High Energy Density Nanocomposites Based on Surface-Modified $BaTiO_3$ and a Ferroelectric Polymer. *ACS Nano* **2009**, *3*, 2581−2592.
(36) Dang, Z. M.; Wang, L.; Yin, Y.; Zhang, Q.; Lei, Q. Q. Giant Dielectric Permittivities in Functionalized Carbon-Nanotube/Electroactive-Polymer Nanocomposites. *Adv. Mater.* **2007**, *19*, 852−857.
(37) Terao, T.; Zhi, C.; Bando, Y.; Mitome, M.; Tang, C.; Golberg, D. Alignment of Boron Nitride Nanotubes in Polymeric Composite Films for Thermal Conductivity Improvement. *J. Phys. Chem. C* **2010**, *114*, 4340−4344.
(38) Kong, P. C.; Pfender, E. Formation of Ultrafine Beta-Silicon Carbide Powders in an Argon Thermal Plasma-Jet. *Langmuir* **1987**, *3*, 259−265.
(39) Meyyappan, M. Plasma Nanotechnology: Past, Present and Future. *J. Phys. D: Appl. Phys.* **2011**, *44*, 174002.
(40) Shigeta, M.; Murphy, A. B. Thermal Plasmas for Nanofabrication. *J. Phys. D: Appl. Phys.* **2011**, *44*, 174025.
(41) Petermann, N.; Stein, N.; Schierning, G.; Theissmann, R.; Stoib, B.; Brandt, M. S.; Hecht, C.; Schulz, C.; Wiggers, H. Plasma Synthesis of Nanostructures for Improved Thermoelectric Properties. *J. Phys. D: Appl. Phys.* **2011**, *44*, 174034.
(42) Nebol'sin, V.; Shchetinin, A. Role of Surface Energy in the Vapor−Liquid−Solid Growth of Silicon. *Inorg. Mater.* **2003**, *39*, 899−903.
(43) Gu, H. B.; Tadakamalla, S.; Huang, Y. D.; Coloradc, H. A.; Luo, Z. P.; Haldolaarachchige, N.; Young, D. P.; Wei, S. Y.; Guo, Z. H. Polyaniline Stabilized Magnetite Nanoparticle Reinforced Epoxy Nanocomposites. *ACS Appl. Mater. Interfaces* **2012**, *4*, 5613−5624.
(44) Schadler, L. S.; Kumar, S. K.; Benicewicz, B. C.; Lewis, S. L.; Harton, S. E. Designed Interfaces in Polymer Nanocomposites: a Fundamental Viewpoint. *MRS Bull.* **2007**, *32*, 335−340.
(45) Nair, C. P. R.; Bindu, R. L.; Ninan, K. N. Thermal Characteristics of Addition-Cure Phenolic Resins. *Polym. Degrad. Stab.* **2001**, *73*, 251−257.
(46) Wang, J. G.; Jiang, H. Y.; Jiang, N. Study on the Pyrolysis of Phenol-Formaldehyde (PF) Resin and Modified PF Resin. *Thermochim. Acta* **2009**, *496*, 136−142.
(47) Chen, Y. F.; Chen, Z. Q.; Xiao, S. Y.; Liu, H. B. A Novel Thermal Degradation Mechanism of Phenol-Formaldehyde Type Resins. *Thermochim. Acta* **2008**, *476*, 39−43.
(48) Trick, K. A.; Saliba, T. E. Mechanisms of the Pyrolysis of Phenolic Resin in a Carbon/Phenolic Composite. *Carbon* **1995**, *33*, 1509−1515.
(49) Gu, H. B.; Tadakamalla, S.; Zhang, X.; Huang, Y. D.; Jiang, Y.; Colorado, H. A.; Luo, Z. P.; Wei, S. Y.; Guo, Z. H. Epoxy Resin Nanosuspensions and Reinforced Nanocomposites from Polyaniline Stabilized Multi-Walled Carbon Nanotubes. *J. Mater. Chem. C* **2013**, *1*, 729−743.
(50) Chen, Y.; Tao, J.; Li, S.; Khashab, N. M. Compositing Polyetherimide with Polyfluorene Wrapped Carbon Nanotubes for Enhanced Interfacial Interaction and Conductivity. *ACS Appl. Mater. Interfaces* **2014**, *6*, 9013−9022.
(51) Khare, K. S.; Khabaz, F.; Khare, R. Effect of Carbon Nanotube Functionalization on Mechanical and Thermal Properties of Cross-Linked Epoxy-Carbon Nanotube Nanocomposites: Role of Strengthening the Interfacial Interactions. *ACS Appl. Mater. Interfaces* **2014**, *6*, 6098−6110.
(52) Kochetov, R.; Korobko, A. V.; Andritsch, T.; Morshuis, P. H. F.; Picken, S. J.; Smit, J. J. Modelling of the Thermal Conductivity in Polymer Nanocomposites and the Impact of the Interface between Filler and Matrix. *J. Phys. D: Appl. Phys.* **2011**, *44*, 395401.
(53) Ishida, H.; Rimdusit, S. Very High Thermal Conductivity Obtained by Boron Nitride-Filled Polybenzoxazine. *Thermochim. Acta* **1998**, *320*, 177−186.
(54) Li, Y.; Huang, X. Y.; Hu, Z. W.; Jiang, P. K.; Li, S. T.; Tanaka, T. Large Dielectric Constant and High Thermal Conductivity in Poly(vinylidene fluoride)/Barium Titanate/Silicon Carbide Three-Phase Nanocomposites. *ACS Appl. Mater. Interfaces* **2011**, *3*, 4396−4403.
(55) Luo, S. B.; Yu, S. H.; Sun, R.; Wong, C. P. Nano Ag-Deposited $BaTiO_3$ Hybrid Particles as Fillers for Polymeric Dielectric

DOI: 10.1021/am5081887
ACS Appl. Mater. Interfaces 2015, 7, 2873−2881

Composites: toward High Dielectric Constant and Suppressed Loss. *ACS Appl. Mater. Interfaces* **2014**, *6*, 176−182.
(56) Wang, G. S. Enhanced Dielectric Properties of Three-Phase-Percolative Composites Based on Thermoplastic-Ceramic Matrix ($BaTiO_3$ + PVDF) and ZnO Radial Nanostructures. *ACS Appl. Mater. Interfaces* **2010**, *2*, 1290−1293.
(57) Zhang, L.; Shan, X. B.; Wu, P. X.; Cheng, Z. Y. Dielectric Characteristics of $CaCu_3Ti_4O_{12}$/P(VDF-TrFE) Nanocomposites. *Appl. Phys. A: Mater. Sci. Process.* **2012**, *107*, 597−602.
(58) Jonscher, A. In *The Universal Dielectric Response, Electrical Insulation and Dielectric Phenomena*, 1990 Annual Report, Conference on, IEEE: New York, 1990; 23−40.
(59) Huang, X.; Zhi, C.; Jiang, P.; Golberg, D.; Bando, Y.; Tanaka, T. Temperature-Dependent Electrical Property Transition of Graphene Oxide Paper. *Nanotechnology* **2012**, *23*, 455705.
(60) Chu, B.; Zhou, X.; Ren, K.; Neese, B.; Lin, M.; Wang, Q.; Bauer, F.; Zhang, Q. A Dielectric Polymer with High Electric Energy Density and Fast Discharge Speed. *Science* **2006**, *313*, 334−336.
(61) Fillery, S. P.; Koerner, H.; Drummy, L.; Dunkerley, E.; Durstock, M. F.; Schmidt, D. F.; Vaia, R. A. Nanolaminates: Increasing Dielectric Breakdown Strength of Composites. *ACS Appl. Mater. Interfaces* **2012**, *4*, 1388−1396.
(62) Nelson, J. K.; Fothergill, J. C. Internal Charge Behaviour of Nanocomposites. *Nanotechnology* **2004**, *15*, 586.
(63) Flandin, L.; Vouyovitch, L.; Beroual, A.; Bessède, J. L.; Alberola, N. Influences of Degree of Curing and Presence of Inorganic Fillers on the Ultimate Electrical Properties of Epoxy-Based Composites: Experiment And Simulation. *J. Phys. D: Appl. Phys.* **2005**, *38*, 144.

DOI: 10.1021/am5081887
ACS Appl. Mater. Interfaces 2015, 7, 2873−2881